POLITECNICO DI TORINO
Repository ISTITUZIONALE

Sensorless standstill commissioning of synchronous reluctance machines with automatic tuning

*Original*
Sensorless standstill commissioning of synchronous reluctance machines with automatic tuning / Pescetto, P., Pellegrino, G.-.M.L.. - (2017), pp. 1-8. (Electric Machines and Drives Conference (IEMDC), 2017 IEEE International Miami, FL, USA 21-24 May 2017) [10.1109/IEMDC.2017.8002302].

*Availability:*
This version is available at: 11583/2679725 since: 2018-02-20T10:08:54Z

*Publisher:*
IEEE

*Published*
DOI:10.1109/IEMDC.2017.8002302

*Terms of use:*

This article is made available under terms and conditions as specified in the corresponding bibliographic description in the repository

*Publisher copyright*

(Article begins on next page)

19 November 2026

# Sensorless Standstill Commissioning of Synchronous Reluctance Machines with Automatic Tuning

Paolo Pescetto[1], Gianmario Pellegrino[1]
[1]Energy department, Politecnico di Torino, Turin, Italy, paolo.pescetto@polito.it

***Abstract*—This paper deals with the sensorless self-commissioning of synchronous reluctance motors at standstill. Previous work demonstrated that the injection of high test voltage pulses can be successfully used to determine the flux linkage maps of the Synchronous Reluctance machine without position transducer and with no need of rotor locking. In this work, the tuning aspects of the above self-commissioning technique are analyzed for making it self-tuning. A method for detecting unwanted rotor movement during the test is introduced and used to assess the test's end and to maximize the $i_d$, $i_q$ area of inspection. Furthermore, the paper analyzes a number of theoretical and practical implementation issues, first mathematically and then in experiments. The effects of possible error sources are evaluated, including imprecise estimation of the stator resistance and of the inverter voltage distortion, and iron loss. Experimental results are presented for three Synchronous Reluctance motor prototypes.**

***Keywords—Magnetic Model Identification; Self-Commissioning; Synchronous Reluctance Motor; Flux Maps; Magnetization Curves***

## I. Introduction

AC Synchronous Motor drives are progressively replacing Induction Motors (IM) drives in a growing number of applications [1], mostly due to their higher efficiency and compactness. Among those electrical machines, the Synchronous Reluctance Machine (SyRM) offers a very good trade-off between performance and low manufacturing cost. The downside is that the identification of the machine's parameters, and namely of the flux maps, is non-obvious and non-standardized. In addition, the replacement of the IM with the SyRM in variable speed applications imposes that the latter is sensorless controlled, and that such sensorless control is easy to calibrate and possibly self-calibrated at the drive installation. From this standpoint, the accurate knowledge of the machine parameters becomes even more important.

The literature reports several techniques for the identification of the flux maps or the inductance maps of synchronous machines [2]-[6]. Most of those techniques require the presence of a position sensor and specific additional hardware such as voltage transducers or a speed-controlled dynamometer machine. Square-wave voltage excitation at standstill was first proposed in [7] for interior permanent magnet machines (IPM) with locked rotor having a position transducer, and using low test voltages. More recently, the technique was improved in [8],[9] specifically for SyR machines, with the introduction of high test voltages and sensorless implementation. The identification is performed at standstill and free-shaft, which is the worst-case condition for self-commissioning. This technique demonstrated to be accurate, robust towards stator resistance and inverter nonlinearities detuning, and encoderless.

The object of this work is to address the several implementation issues of the flux curves identification technique presented in [9], by investigating the underpinning theory and proposing solutions for tuning automation. Above all, the rotor has not to move during the test, even in free-shaft conditions. Depending on the aggregate of applied voltages, current levels and rotor inertia, such lack of movement can be hard to guarantee. In this work, an automatic method to detect rotor movements is proposed, capable of assessing the goodness of the identification test. Based on this, an automatic tuning procedure of the peak voltage and current levels is formulated and tested. Finally, three possible error sources are analyzed in detail. The effects of inaccurate knowledge of the motor stator resistance and of the inverter voltage error are quantified, as well as the effect of iron loss on the final magnetic curves. All the results are supported by experimental tests on three SyRMs motor prototypes.

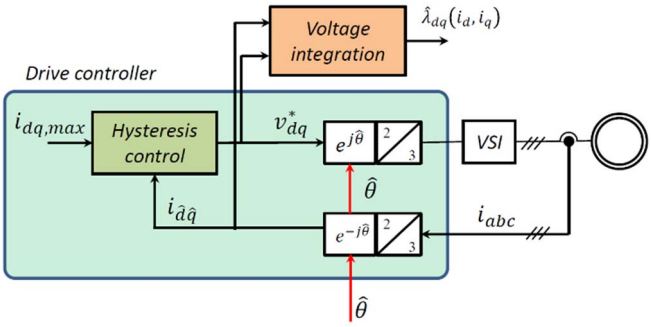



Fig. 1. Block diagram decribing the self-commissioning procedure [9]. Test#1 explores the *d* axis, Test#2 the *q* axis and Test#3 both the *d* and *q* axes.

## II. Square Wave Voltage Sensorless Method

The sensorless self-commissioning method is described in Fig. 1. The motor shaft is free and there is no position transducer. Before the test, the rotor position estimate $\hat{\theta}$ is determined by means of a saliency based sensorless technique (e.g. pulsating or rotating high frequency voltage injection). Alternatively, the rotor position can be imposed by exciting the machine with direct current (rotor parking). It is assumed that the rotor does not move during the test, so such initial position $\hat{\theta}$ used for *dq* coordinates definition is retained during the flux curves identification.

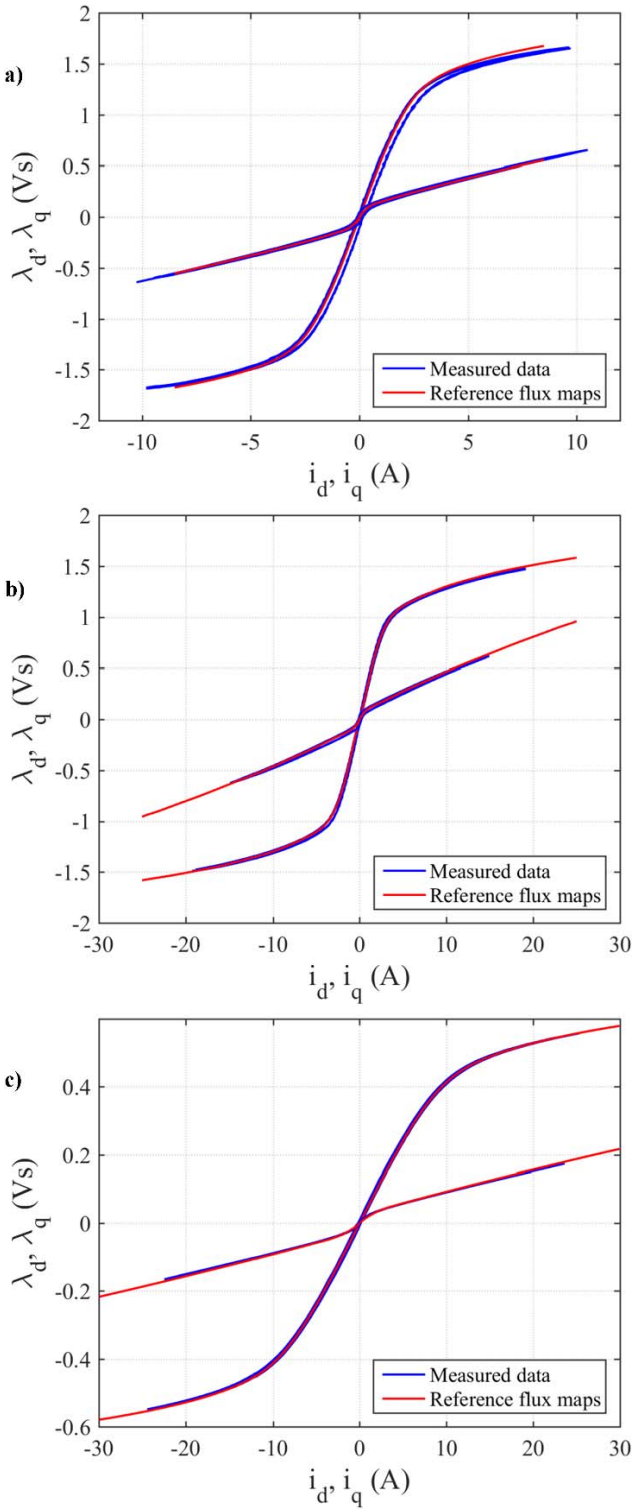



Fig. 2. Magnetic model identification (test #1 and test #2). The resistive voltage drop and the inverter nonlinear effects are accurately compensated.The reference curves (red) are obtained according to [6]. a) motor #1; b) motor #2; c) motor #3.

Exploiting the complex notation, the flux linkage vector $\bar{\lambda}_{dq}$ at standstill is (1):

$$\bar{\lambda}_{dq} = \int \left(\bar{v}_{dq} - R_s \bar{\imath}_{dq}\right) dt \tag{1}$$

Where $\bar{v}_{dq}$ and $\bar{\imath}_{dq}$ are the voltage and current vectors and $R_s$ is the stator resistance.

The motor commissioning procedure is divided in 3 phases, called Test #1, #2 and #3.

**Test #1**: the $d$ axis is excited with a bipolar square-wave voltage $v_d^*$, reversing its polarity whenever the absolute value of $i_d$ overcomes a defined threshold value $i_{d,max}$. Meanwhile, $v_q^*$ is set to 0. Respect to (1), in this implementation the position of the $d$ axis is estimated (i.e. $\hat{d}\hat{q}$ coordinates are used in place of $dq$ ones), and the motor voltages are estimated via the inverter voltage commands, indicated with a star superscript.

In this way, the $d$ axis magnetic characteristic $\hat{\lambda}_d(i_d, i_q = 0)$ is evaluated as:

$$\hat{\lambda}_{\hat{d}} = \int \left(v_{\hat{d}}^* - V_{th} sign(i_{\hat{d}}) - \hat{R}_s i_{\hat{d}}\right) dt \tag{2}$$

where $\hat{R}_S$ is the stator resistance estimate, and $\hat{V}_{th}$ is the estimated amplitude of the inverter voltage distortion term [10].

**Test #2**: the same procedure is applied to the $q$-axis, with $v_d^* = 0$, to evaluate $\hat{\lambda}_q(i_d = 0, i_q)$:

$$\hat{\lambda}_{\hat{q}} = \int \left(v_{\hat{q}}^* - V_{th} sign(i_{\hat{q}}) - \hat{R}_s i_{\hat{q}}\right) dt \tag{3}$$

**Test #3**: the two axes are excited at the same time, and each axis' voltage is reversed according to the respective current's limit. This latter test add information about cross-saturation to the single axis curves $\hat{\lambda}_d(i_d), \hat{\lambda}_q(i_q)$ identified through (2) and (3). Details can be found in [9].

Tests are reported for three SyR motors, whose ratings are reported in TABLE I. The single-axis characteristics obtained from Tests #1 and #2 are compared with the reference flux maps (measured at constant speed according to [6]) in Fig. 2 for the three motors. It can be noticed that the self commissioning test allowed to characterize each motor up to currents considerably higher than the rated value.

TABLE I. RATINGS OF THE MOTORS UNDER TEST

| | Motor #1 | Motor #2 | Motor #3 |
|---|---|---|---|
| Nominal current RMS [A] | 2.8 | 5.08 | 17.5 |
| Nominal voltage RMS [V] | 408 | 400 | 400 |
| Pole pairs | 2 | 2 | 3 |
| Nominal torque [Nm] | 7.1 | 15 | 37.5 |
| Nominal speed [rpm] | 1479 | 1400 | 1000 |
| Nominal power [kW] | 1.1 | 2.2 | 3.97 |
| Phase resistance [Ohm] | 4.59 | 3.58 | 0.42 |

## III. Analysis of Identification Errors

### A. Detuning of the Stator Resistance

The stator resistance can be measured just before the test through direct current injection. Since the flux identification procedure duration is in the order of some seconds, the windings temperature will not have time to vary and the same will be true for $\hat{R}_s$ in (2) and (3). Nevertheless, if $R_s$ is misestimated for some reason, the flux estimate error $\epsilon_{\lambda,Rs}$ is proportional to the resistance detuning and to the integral of the current (Fig. 3b):

$$\varepsilon_{\lambda,Rs} = \left(\hat{R}_s - R_s\right) \int i_d dt \tag{4}$$

The detuning error $\hat{R}_s - R_s$ produces a loop of increased amplitude in the $i_d, \lambda_d$ plane, as shown by in Fig. 3d), where the case of 100% detuning ($\hat{R}_s = 0$) is reported. The detuning effect can be easily compensated by averaging the hysteresis loop. Fig. 3d) shows that even with 100% detuning the average between the high and low curves of the black loop is very close to the same average applied to the red loop, where $\hat{R}_s = R_s$.

As known, the magnetizing transient is always faster than the demagnetization because of the voltage drop on $R_s$. This phenomenon produces an asymmetry in the cycle, so the error term computed in (4) is not null at the voltage reversal, as can be seen in Fig. 3b). For this reason, the detuned average $\lambda_d(i_d)$ curve is slightly shifted respect to the correct characteristic for high current, close to the imposed limit $i_{d,max}$.

### B. Inverter Voltage Error

Inaccurate compensation of inverter nonlinearities produces a similar effect (5).

$$\epsilon_{\lambda,Vth} = \int \left(\hat{V}_{th} - V_{th}\right) \cdot sign(i_d)\ dt \tag{5}$$

Detuning of the inverter error compensation term $\hat{V}_{th}$ produces a triangular flux error waveform $\epsilon_{\lambda,Vth}$ proportional to the compensation detuning (Fig. 3c). As can be seen in Fig. 3e), the effects on the estimated flux (thickness of the loop and shift at high current) are similar to error $\varepsilon_{\lambda,Rs}$. Also in this case, even with 100% detuning ($\hat{V}_{th} = 0$) the error on identified flux is low thanks to the high amplitude of the applied square-wave voltage, which is approximately 17 times higher than the inverter distortion voltage $V_{th}$ in the tests.

### C. Discussion

Assuming that $\left(\hat{V}_{th} - V_{th}\right)$ is constant, the time waveform of $\epsilon_{\lambda,Vth}$ is a triangular function (Fig. 3c). Assuming constant inductance, $\epsilon_{\lambda,Rs}$ waveform would be a series of exponential functions. Anyway, because of the magnetic saturation $\epsilon_{\lambda,Rs}$ is a nonlinear waveform. For this reason, it is not obvious to evaluate which term is more significant in practical implementation. Different scenarios are possible depending on the accuracy of $\hat{R}_s$ and $\hat{V}_{th}$. For the motor under test and inverter error, the two error sources have similar peak value (around 0.1 Vs), but $\epsilon_{\lambda,Rs}$ has higher effect both on the loop thickness and shift at high current. This is mainly due to the different time waveform of $\epsilon_{\lambda,Rs}$, where a relatively high error persists for a longer time compared to $\epsilon_{\lambda,Vth}$.

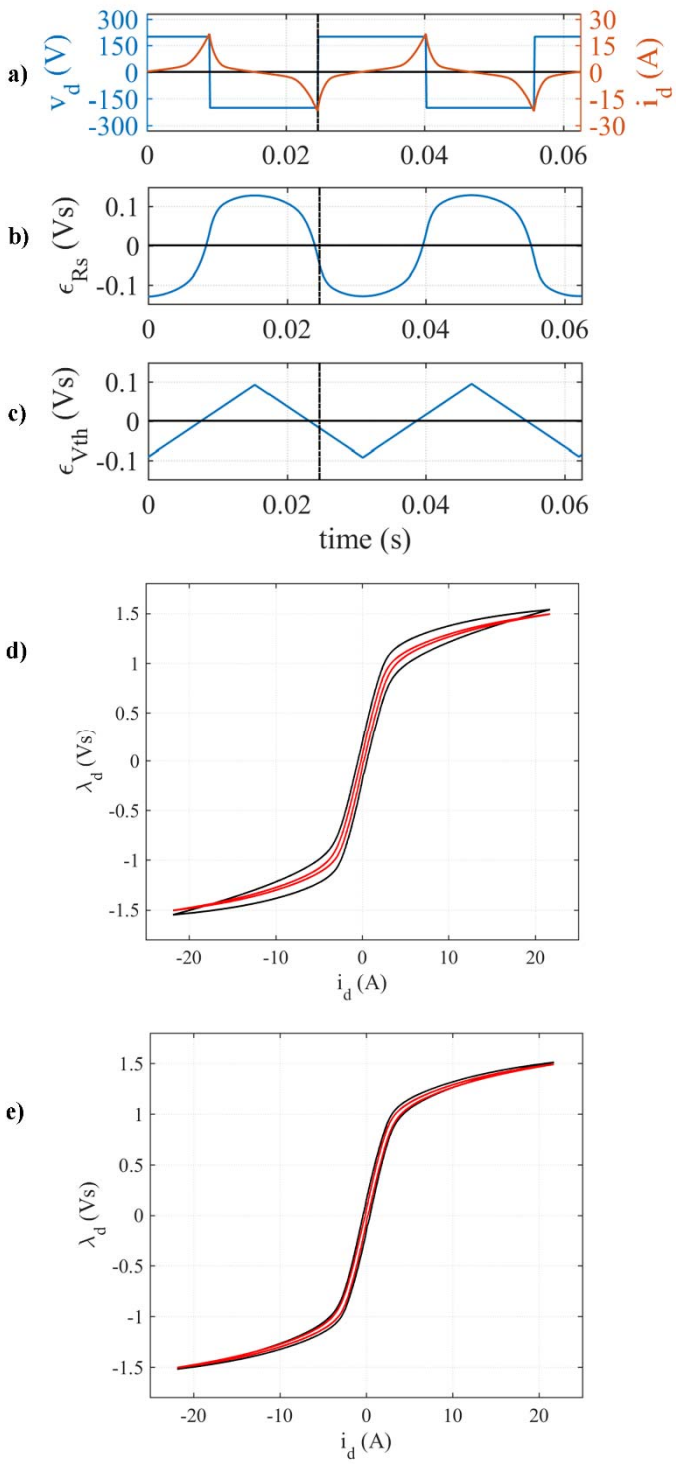



Fig. 3. Test #1 (experimental). a) applied reference voltage and measured current; b) flux error due to $R_s$ inaccuracy ($\hat{R}_s = 0$); c) flux error due to inverter nonlinearities ($\hat{V}_{Th} = 0$); d) Estimated flux characteristic with (red) and without (black) compensating the voltage drop on $R_s$. e) Estimated flux characteristic with (red) and without (black) compensating the inverter voltage drop $V_{Th}$.

It must be considered the 100% detuning case presented in Fig. 3 is an hyper worst case scenario, at least for $\hat{R}_s$. It is very unlikely that in real applications the resistance is completely

unknown. More likely, the resistance value will be badly known (i.e. at the wrong temperature) and the deviation of the flux estimate would be much lower than the presented one.

In conclusion, the higher is the amplitude of the applied voltage, the lower will be the sensitivity of the magnetic curves to both the detuning of $\hat{R}_s$ and $\hat{V}_{th}$.

*D. Iron Loss*

Information about iron loss can be extracted from the current samples collected during flux identification. Eddy current- and hysteresis losses affect the shape of the flux loop. Fig. 4 shows the current discontinuity at each positive and negative peak, in occasion of voltage reversals.

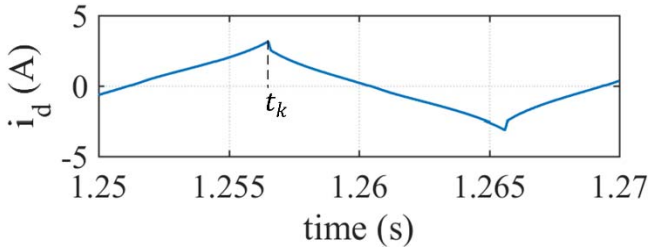



Fig. 4. Iron losses effect on stator current $i_d$ during test #1 (simulation).

This behavior is consistent with the presence of iron losses, modeled as a resistance $R_{Fe}$ in parallel to the induced stator voltage (Fig. 5). Therefore, a resistive current proportional to the applied induced voltage is superimposed to the inductive current.

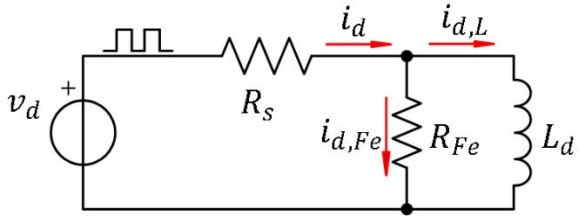



Fig. 5. Simplified eqivalent circuit including iron losses.

Using the simple model of Fig. 5, and considering a square wave excitation of the d-axis as in *test #1*, the following equations can be obtained:

$$i_d = i_{d,L} + i_{d,Fe} \tag{6}$$

Where $i_{d,L}$ and $i_{d,Fe}$ are the current components passing through the equivalent inductance and the equivalent iron resistance, respectively. Considering the sampling time $t_k$ as the instant when the voltage polarity is reversed, as in Fig. 4, the following quantities are defined:

$$i_d(k-0.5) = \frac{i_d(k-1)+i_d(k)}{2} \tag{7}$$

$$i_d(k+0.5) = \frac{i_d(k)+i_d(k+1)}{2} \tag{8}$$

It is assumed that the current in the inductance $i_{d,L}$ does not considerably change between the sampling instant $(k-1)$ and $(k+1)$, therefore the value of the apparent inductance $L_d$ can be calculated before the voltage reversal and it is used as constant:

$$L_d = \frac{V - R_s i_d(k-0.5) - V_{th}}{i_d(k) - i_d(k-1)} T_s \tag{9}$$

Where $V$ is the amplitude of the applied reference voltage and $T_s$ is the sampling period. The inductive and resistive current components at the sampling time $(k-1)$ can be respectively computed as:

$$i_{d,L}(k-1) = i_{d,L}(k) - \frac{V - R_s i_d(k-0.5) - V_{th}}{L_d} T_s \tag{10}$$

$$i_{d,Fe}(k-1) = \frac{V - R_s i_d(k-1) - V_{th}}{R_{Fe}} \tag{11}$$

While, at the sampling time $(k+1)$:

$$i_{d,L}(k+1) = i_{d,L}(k) + \frac{-V - R_s i_d(k+0.5) - V_{th}}{L_d} T_s \tag{12}$$

$$i_{d,Fe}(k+1) = \frac{-V - R_s i_d(k+1) - V_{th}}{R_{Fe}} \tag{13}$$

After a straightforward manipulation of (6)-(13), $R_{Fe}$ can be estimated as:

$$\hat{R}_{Fe} = \frac{2V - R_s\left(i_d(k-1) - i_d(k+1)\right)}{i_d(k-1) - i_d(k+1) - \frac{T_s}{L_d}\left[R_s\left(i_d(k-0.5) + i_d(k+0.5)\right) + 2V_{Th}\right]} \tag{14}$$

In turn, the iron loss circuital term $R_{Fe}$ can be determined by manipulation of the current samples during the motor commissioning. This technique resulted accurate in simulations (Fig. 4), where a constant value of resistance was used to represent the iron loss effect. Anyway, it must be considered that such model is a simplified representation made for steady state conditions, whereas the iron losses provoked by step voltage transients might behave differently. So far, it was not possible to validate the $R_{Fe}$ estimation (14) experimentally, and obtain results that are comparable to those of iron loss determination via dynamometer tests. This phenomenon is still under investigation.

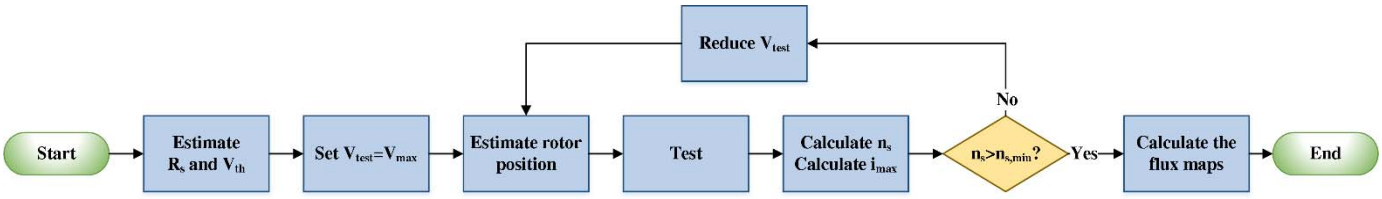



Fig. 6. Test sequence flow chart for the magnetic model identification with automatic tuning.

## IV. Automatic Tuning Procedure

### A. Automatic Selection of the Voltage Amplitude

As said, the higher is the excitation voltage used in the tests, the lower is the effect of detuning, since the resistance voltage drop and the inverter voltage error become less important in percentage.

Also, applying a high $v_d^*$ and/or $v_q^*$ increases the frequency at which the current is reversed, i.e. it makes the machine excitation and de-excitation transients quicker, increasing the likelihood that the rotor remains at standstill during the test. This is particularly critical in test #3, when both axes are excited and torque reaches high transient values that tend to accelerate the rotor. If the torque polarity is reversed at a sufficiently high rate, it is easier to avoid unwanted movement. The downside is that a high $v_d^*$ or $v_q^*$ can result in a reduced number of current (and flux) samples per period.

The suggested good practice is to use a test voltage amplitude equal to the maximum inverter voltage $V_{test} = V_{max}$ to minimize the risk of rotor movement and the effects of $(\hat{R}_s, \hat{V}_{th})$ detuning, and then check if the obtained number of samples per period $n_s$ is adequate (e.g. $n_{s,min} = 100$). If $n_s < n_{s,min}$ the test is repeated with a lower test voltage, at the cost of slightly increased detuning sensitivity and risk of movement. The procedure can be run automatically, according to the flow chart presented in Fig. 6.

### B. Automatic Selection of the Current Limits

In principle, the area of identification of the flux maps in the current plane $i_d, i_q$ should be as large as possible, covering current values well beyond the machine's rated current. This is not always possible, because of the tendency of the rotor to spin away, when high current levels are applied. In this respect, the three tests behave quite differently. For test #1, the current limit $i_{d,max}$ can be set as high as desired. When the *d* axis is excited torque is zero, and there is no risk of movement. Furthermore, even in case of an unwanted initial misalignment, the produced torque tends to align the rotor to the correct *d* position.

Conversely, when the estimated *q* axis is excited (test #2), any minimum rotor misalignment produces a torque that increases the position error, corrupting the flux curve identification and eventually moving the rotor off position. In this test, if the rotor slightly moves the position error diverges and the shaft starts to rotate. The choice of $i_{q,max}$, has direct effect on the magnitude and duration of the misalignment torque: if $i_{q,max}$ is too high, the friction is overcome and movement is non-negligible.

Finally, the cross-saturation test #3 is where transient torque is inherently produced by the concurrent presence of $i_d$ and $i_q$ current components. The rotor movement can be avoided if torque reversals are fast, and the choice of the $i_{d,max}$ and $i_{q,max}$ for this test is the most challenging of all. The maximum achievable current is not known a priori, and depends on many factors such as the Nm/Ampere capability of the motor, its inertia and friction.

This paper proposes to use high values of $i_{d,max}$, intended as higher than necessary to just cover the operating area of the motor, both for tests #1 and #3, because this tends to align and stabilize the rotor. The limit $i_{q,max}$ in tests #2 and #3 is found iteratively starting from very low values and increasing the limit progressively until the rotor moves. The test is stopped when rotor movement is detected, meaning that the maximum possible $i_q$ has been reached. Movement is sensorless detected as described in the next section.

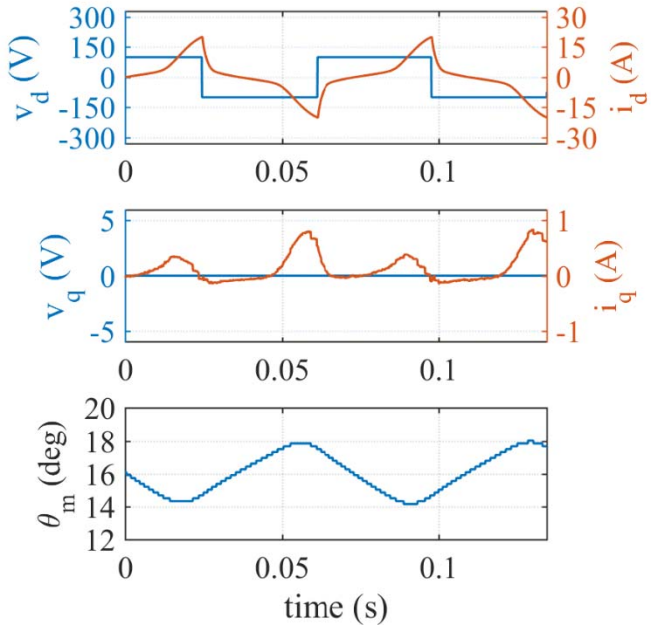



Fig. 7. Test #1 (experimental); $v_d^* = 100\,V$. From top to bottom: voltage and current on d axis; voltage and current on q axis; mechanical position

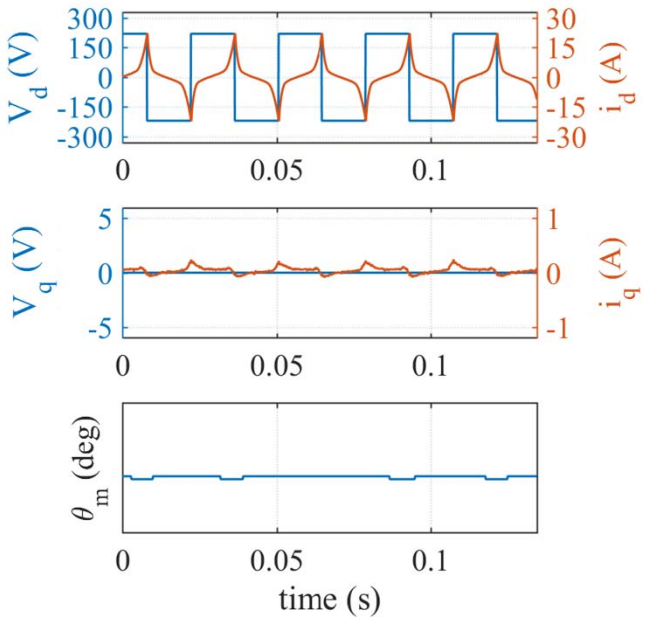



Fig. 8. Test #1 (experimental): $v_d^* = 200\,V$. From top to bottom: voltage and current on d axis; voltage and current on q axis; mechanical position.

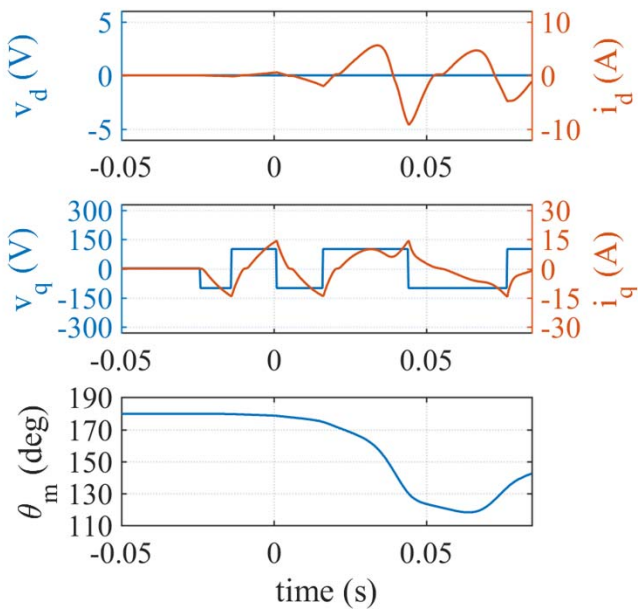



Fig. 9. Test #2 (experimental): between $v_q^* = 100\,V$. From top to bottom: voltage and current on d axis; voltage and current on q axis; mechanical position.

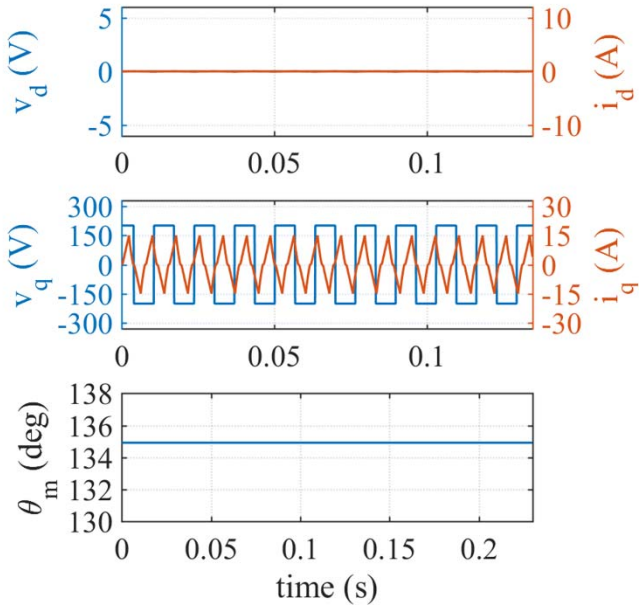



Fig. 10. Test #2 (experimental): $v_q^* = 200\,V$. From top to bottom: voltage and current on d axis; voltage and current on q axis; mechanical position.

### C. Detection of Movement

Test #1 is self-aligning, as said. Two methods are proposed to detect rotor misalignment for tests #2 and #3. In test #2 the $q$ axis alone is excited. Therefore, zero current in the estimated $\hat{d}$ axis is expected. If the motor shifts from the correct position, the non-zero current value on the $\hat{d}$ axis is used as a position error information. When, during a $q$ axis identification test, the $i_{\hat{d}}$ signal is consistently shifted from zero, the test is stopped and the data referring to the last $i_{q,max}$ value are cancelled.

For test #3, when both axis are excited, a movement detection signal is artificially built by observing whether the $i_d$ waveform is monotonic during one voltage pulse. If not, it means that the rotor position is varying significantly, and the rotor will eventually start to rotate. Therefore, if the $i_d$ derivative is not in accordance with the applied voltage the movement detection feedback is increased by one at each sampling time. The movement detection feedback represents an approximation of the position error accumulated during one sweep of the $d$ axis current. The test is stopped if the error signal overcomes a defined threshold value. If not, the movement detection feedback is reset after each half cycle of the $d$ axis voltage. This technique is new to the literature. The tuning of the tripping threshold is described in Section V, alongside the results.

## V. Experimental Results

The magnetic model identification described in chapter II has been tested on three SyR motor prototypes, as shown in Fig. 2. Then, the motor #2 has been used to validate the novel contribution described in section III and IV.

### A. Effect of the Test Voltage Amplitude

Tests #1 and #2 were experimentally performed on varying the amplitude of the applied voltage. In Fig. 7 and Fig. 8, the $d$ axis was excited with $v_d^* = 100\,V$ and $200\,V$ respectively in two separate tests. As said in Section IV.A, the latter test resulted more accurate and stable, with lower position error and current on the $q$ axis. Then, in Fig. 9 and Fig. 10, the $q$ axis was tested, again applying $v_q^* = 100\,V$ and later $v_q^* = 200\,V$ respectively. As can be seen, the first test failed and the rotor moved from its initial position, while increasing the test voltage the system resulted stable and position oscillations were avoided. The number of samples is sufficient in both cases (284 and 133 samples per cycle in the tests of Fig. 8 and Fig. 10 respectively).

### B. Validation of Movement Detection Techniques

The techniques proposed in section IV.B and IV.C have been experimentally tested. In Fig. 11, the $q$ axis is tested linearly increasing $i_{q,max}$ limit. The test is stopped when $i_d$ exceeds a certain limit, used to indicate rotor movement. Dealing with the tuning of such $i_d$ threshold, the test was repeated several times using different threshold values. The results highlight that the value used for $i_d$ threshold is not important, since when the rotor moves from its initial position it then immediately starts to rotate, producing detectable current in the estimated $\hat{d}$ axis. In Fig. 11, two tests are compared. The first (left) has been stopped when $i_d$ reached 1 A, while in the second (right) the threshold value has been set at 2 A. In both the cases, the maximum $i_q$ reached approximately the same value ($i_{q,max} = 9.07\,A$ and $i_{q,max} = 9.22\,A$ in the two tests), proving the robustness of the method towards the choice of the $i_d$ threshold.

Finally, in Fig. 12 and Fig. 13 the cross-saturation test has been experimentally verified linearly increasing $i_{q,max}$, with different values of constant $i_{d,max}$. The rotor movement is detected through the analysis of the $i_d$ derivative. As said, the test stopped if the current derivative is not coherent with the sign of the applied $v_d$ for a sufficient number of samples, indicated by the *movement detection feedback*. The threshold value for

such detection signal (called *"Movement"* in the figures) has to be tuned. The test has been repeated several times varying the applied $i_{d,max}$ limit (constant during each test) and the movement detection threshold, aiming at maximizing the feasible $i_{q,max}$.

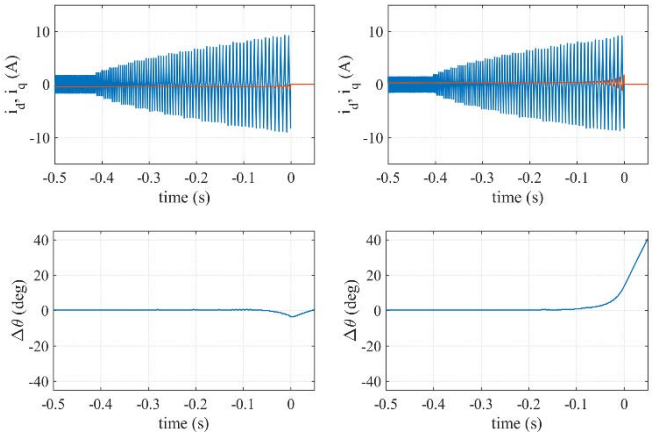



Fig. 11. Test #2 with position detection. Each test has been automatically stopped for $i_d = 1\ A$ (left) and for for $i_d = 2\ A$ (right)

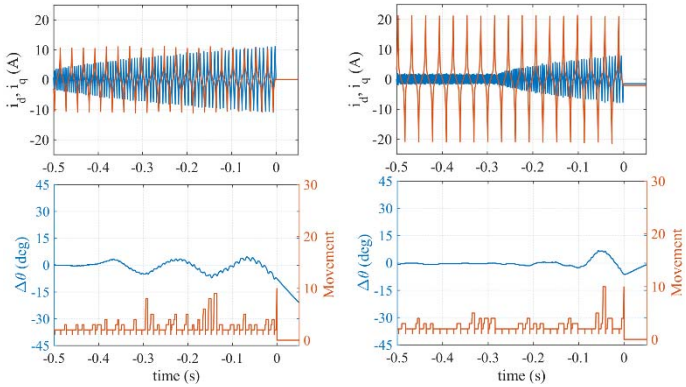



Fig. 12. Test #3 with position detection. Each test has been automatically stopped when the movement feedback reached 10. Left: $i_{d,max} = 10\ A$; right: $i_{d,max} = 20\ A$.

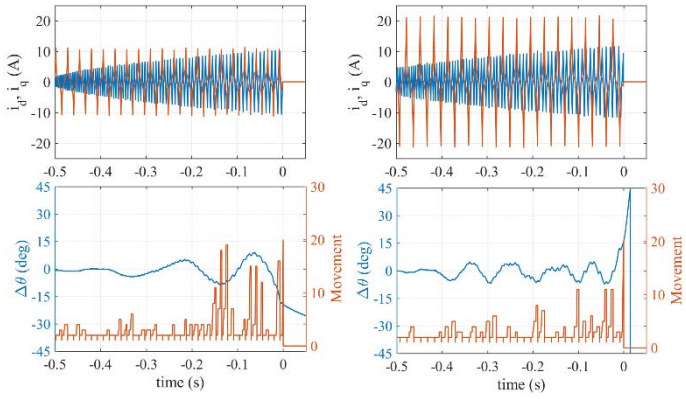



Fig. 13. Test #3 with position detection. Each test has been automatically stopped when the movement feedback reached 20. Left: $i_{d,max} = 10\ A$; right: $i_{d,max} = 20\ A$.

The summary reported in TABLE II. shows that the value of $i_{d,max}$ slightly increases the achieavable $i_{q,max}$. This can be explained considering that higher $i_d$ stabilizes the system, reducing the risk of movement. Nevertheless, for every performed test the most critical condition, detected with highest current distortion, resulted when $i_q$ is close to the limit $i_{q,max}$ while $i_d$ is low, close to the zero crossing. This situation is the most unstable, and it can randomly occur during the test. This phenomenon reduced the influence of $i_{d,max}$ on the maximum acheaved $i_{q,max}$. In real-world implementation, if one test does not cover a sufficient area in the current plane this will be repeated, until aleatory unfavourable conditions are not met.

Considering the tuning of the best threshold for the movement detection feedback, the relation between the threashold value and the maximum position oscillation is non-linear and hard to find. In the performed tests a good consistency between the threashold value and the position displacement was observed, as can be seen in TABLE II. Also, repeating the tests the maximum acheaved $i_{q,max}$ resulted slightly affected by the variation of the threashold value. Fig. 12 reports the test performed with $i_{d,max}$ from 10 A to 20 A, while the threasold value for the movement detection signal was set to 10. This means that the test was stopped when the sign of $i_d$ derivative was not in accordance with $v_d$ for at least 10 samples in one semi-cycle. In both the tests, the maximum position displacement has been between 6 and 8 mechanical degree. In Fig. 13 the test has been performed, again varying $i_{d,max}$ from 10 A to 20 A, but increasing the admittible movement detection signal to 20. Again, similar maximum position oscillation (between 16 and 20 mechanical degree) was reached.

According to TABLE II. , the maximum reached $i_{q,max}$ variation is very limited (around 11 A), proving the substantial insensitivity to parameter tuning. Aleatory unfavorable conditions randomly occurred in some tests, that were stopped for lower $i_{q,max}$.

The effect of the position error on the accuracy of the obtained flux maps is under investigation.

## VI. Conclusions

The sensorless self-commissioning magnetic model identification for SyR proposed in [9] was experimentally tested on three motor prototypes, resulting accurate and with low detuning sensitivity. Theoretical and experimental analysis of possible error sources is presented, confirming the robustness of the method. Moreover, an investigation on a possible technique to estimate the iron losses using a simplified machine model is presented. The test sequence and tuning procedure was made automatic, improving the applicability of this self-commissioning technique for industrial use. Finally, a method to detect any undesired rotor movement is given, permitting to ensure the success of the test and its complete automatization. The experimental results finely validate the goodness of the proposed technique.

TABLE II. PERFORMANCE OF MOVEMENT DETECTION DURING TEST #3.

| Movement feedback threshold | $i_{d,max}$ [A] | $i_{q,max}$ [A] | $\Delta\theta_{max}$ [mec. deg.] |
|---|---|---|---|
| 10 | 5 | 8.56 | 11.08 |
| | 10 | 11.18 | 7.55 |
| | 15 | 10.51 | 6.16 |
| | 20 | 8.33 | 6.14 |
| 15 | 5 | 9.08 | 12.12 |
| | 10 | 12.21 | 8.97 |
| | 15 | 9.35 | 9.03 |
| | 20 | 11.99 | 13.89 |
| 20 | 5 | 10.45 | 17.76 |
| | 10 | 10.43 | 19.15 |
| | 15 | 11.01 | 12.83 |
| | 20 | 11.74 | 16.12 |
| 25 | 5 | 8.35 | 15.30 |
| | 10 | 11.06 | 18.11 |
| | 15 | 11.80 | 21.63 |
| | 20 | 11.78 | 24.43 |
| 30 | 5 | 9.49 | 18.11 |
| | 10 | 11.74 | 17.04 |
| | 15 | 11.96 | 14.23 |
| | 20 | 11.53 | 24.08 |

## REFERENCES


[1] A. T. de Almeida, F. J. T. E. Ferreira and G. Baoming, "Beyond Induction Motors—Technology Trends to Move Up Efficiency," in *IEEE Transactions on Industry Applications*, vol. 50, no. 3, pp. 2103-2114, May-June 2014.

[2] S. A. Odhano, R. Bojoi, Ş. G. Roşu and A. Tenconi, "Identification of the Magnetic Model of Permanent-Magnet Synchronous Machines Using DC-Biased Low-Frequency AC Signal Injection," in *IEEE Transactions on Industry Applications*, vol. 51, no. 4, pp. 3208-3215, July-Aug. 2015.

[3] D. Uzel and Z. Peroutka, "Optimal control and identification of model parameters of traction interior permanent magnet synchronous motor drive," in *Proc. IEEE IECON 2011*, Melbourne, Australia, Nov. 2011.

[4] S. Ebersberger and B. Piepenbreier, "Identification of differential inductances of permanent magnet synchronous machines using test current signal injection," in *Proc. SPEEDAM 2012*, Sorrento, Italy, June 2012, pp. 1342–1347.

[5] I. Omrane, E. Etien, O. Bachelier, and W. Dib, "A simplified least squares identification of permanent magnet synchronous motor parameters at standstill," in *Proc. IEEE IECON 2013*, Vienna, Austria, Nov. 2013.

[6] E. Armando, R. I. Bojoi, P. Guglielmi, G. Pellegrino and M. Pastorelli, "Experimental Identification of the Magnetic Model of Synchronous Machines," in *IEEE Transactions on Industry Applications*, vol. 49, no. 5, pp. 2116-2125, Sept.-Oct. 2013.

[7] B. Stumberger, G. Stumberger, D. Dolinar, A. Hamler and M. Trlep, "Evaluation of saturation and cross-magnetization effects in interior permanent-magnet synchronous motor," in *IEEE Transactions on Industry Applications*, vol. 39, no. 5, pp. 1264-1271, Sept.-Oct. 2003.

[8] N. Bedetti, S. Calligaro and R. Petrella, "Stand-Still Self-Identification of Flux Characteristics for Synchronous Reluctance Machines Using Novel Saturation Approximating Function and Multiple Linear Regression," in *IEEE Transactions on Industry Applications*, vol. 52, no. 4, pp. 3083-3092, July-Aug. 2016.

[9] M. Hinkkanen; P. Pescetto; E. Molsa; S. E. Saarakkala; G. Pellegrino; R. Bojoi, "Sensorless self-commissioning of synchronous reluctance motors at standstill without rotor locking," in *IEEE Transactions on Industry Applications* , vol.PP, no.99, pp.1-1

[10] S. Bolognani and M. Zigliotto, "Self-commissioning compensation of inverter non-idealities for sensorless AC drives applications," 2002 International Conference on Power Electronics, Machines and Drives (Conf. Publ. No. 487), 2002, pp. 30-37.